Shock-capturing in LES of high-speed flows

By M. P. Martín

1. Motivation and objectives

The bursting events that are present in a turbulent boundary layer bring low-momentum fluid from the near wall region into the boundary layer edge. In high-speed boundary layers, shocks form where the low-momentum fluid meets the incoming free-stream. Thus, to perform accurate large-eddy simulations (LES) of these flows, shock-capturing techniques are necessary.

There are two types of shock-capturing techniques: total variation diminishing (TVD) and essentially nonoscillatory (ENO) schemes. TVD shock-capturing techniques reduce to first-order accuracy near shocks and damp the small-scale flow features. Thus, this type of technique is not desired for turbulent flows. ENO schemes are designed to maintain high-accuracy but not high-bandwidth, which is necessary for performing accurate numerical simulations of turbulent flows. Also, ENO schemes are inherently dissipative due to the upwinded, optimal difference stencils and the smoothness measurement. Recently, Weirs and Candler (1997) designed an optimized ENO scheme for simulating compressible turbulent flows based on the weighted essentially nonoscillatory (WENO) scheme of Jiang and Shu (1996). Weirs and Candler used bandwidth optimization techniques and developed symmetric optimal stencils with reduced dissipation and greater resolving efficiency than those provided by typical ENO schemes. Martín and Candler (2000) show that this WENO scheme gives good results for the direct numerical simulation (DNS) of supersonic turbulent boundary layers.

In the present work, the presence of shock waves in high-speed boundary layers is illustrated and the results from the LES of a supersonic boundary layer using the WENO scheme are assessed.

2. Flow conditions

In the present work we use the perfect gas boundary layer database from the DNS of Martín and Candler (2000) and the LES of Martín *et al.* (2000a). The boundary layer edge conditions are $Re_\theta = 7000$, $M_\infty = 4$, $T_\infty = 5000$ K, and $\rho_\infty = 0.5$ kg/m^3. These conditions represent the boundary layer on a 26 degree wedge at Mach number of 20 and 20 km altitude and are illustrated in Fig. 1.

The numerical method combines a WENO scheme for the inviscid fluxes with an implicit time advancement technique. The third-order accurate, high-bandwidth, WENO scheme was designed for low dissipation (Weirs and Candler, 1997) and provides shock-capturing. The time advancement technique is based on the Data-Parallel Lower-Upper (DPLU) relaxation method of Candler *et al.* (1994), which was extended to second-order accuracy by Olejniczak & Candler (1997). The derivatives required for the viscous terms are evaluated using 4th-order central differences. The subgrid-scale terms appearing in the conservative form of the momentum and total energy equations are described in Martín *et al.* (2000b).

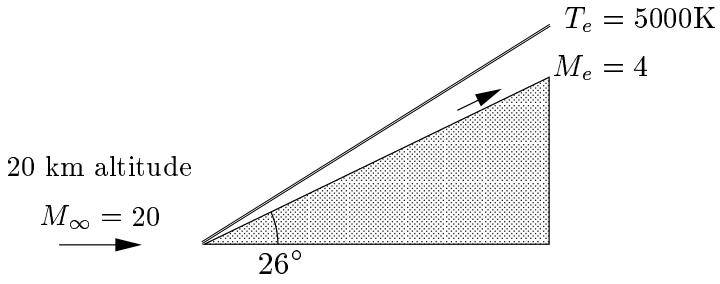

FIGURE 1. Flow conditions.

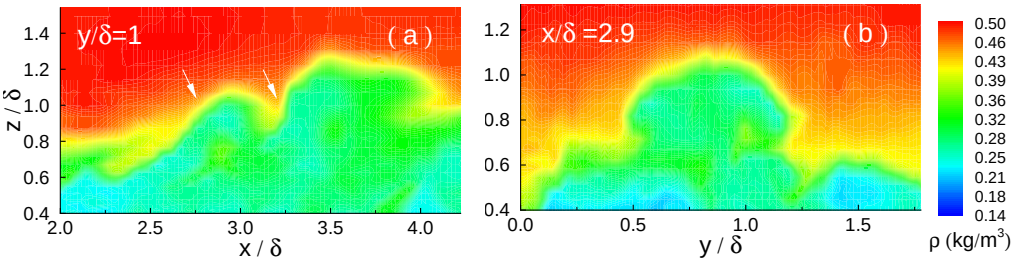

FIGURE 2. Density contours in a (a) streamwise-wall-normal plane and (b) spanwise-wall-normal plane.

3. Results

3.1. *High-speed boundary layer flow physics from DNS*

In this section, the presence of shock waves in high-speed boundary layers is illustrated. Figure 2 shows density contours in streamwise-wall-normal and spanwise-wall-normal planes, respectively. The large-scale bursting events cause strong density gradients near the boundary layer edge. Figure 2b illustrates the three-dimensional character of the strong compression regions. To determine the presence of shock waves, the entropy and pressure changes along a streamline that cross the strong density gradients are considered. The non-isentropic flow condition and a pressure jump are necessary conditions for a shock to occur. Thus, the isentropic and constant pressure relations given by

$$\frac{\rho'}{\langle\rho\rangle_v} = (\gamma - 1)\frac{T'}{\langle T\rangle_v} \,, \tag{3.1}$$

$$\frac{\rho'}{\langle\rho\rangle_v} = -\frac{T'}{\langle T\rangle_v} \,, \tag{3.2}$$

must not be met across the shock, where $\langle\rho\rangle_v$ and $\langle T\rangle_v$ are the average density and temperature in the volume that encloses the streamline. Figure 3 shows a scatter plot of the normalized density and temperature fluctuations along the streamline crossing the strong gradients shown in Fig. 2a. The solid line represents the isentropic flow relation. The dashed line represents the constant pressure condition. A turbulence field is non-conservative, thus we do not expect that the data will line up along the solid line. As it can be seen in Fig. 3, the flow is not isentropic. For the most part, the fluid particle follows a constant pressure path. However, the red symbols show that somewhere along the streamline the flow undergoes a pressure change. Jumps in the density, temperature,

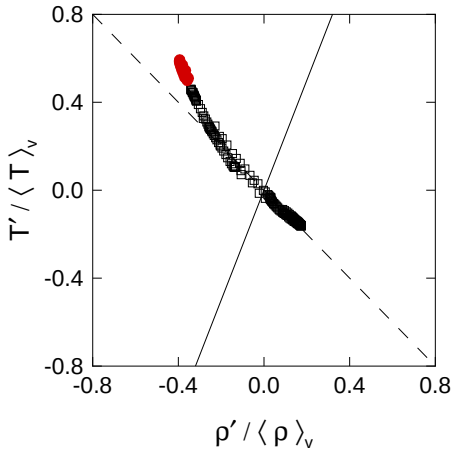

FIGURE 3. Scatter plot of the normalized temperature and density fluctuations along the flow-particle path across the density gradients shown in Fig. 2. Symbols, DNS data; ——— , isentropic relation; – – – , constant pressure relation.

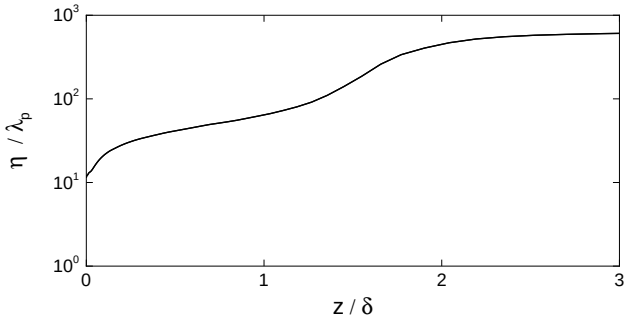

FIGURE 4. Ratio of the Kolmogorov scale to the molecular mean free path.

and dilatation are also associated with the red symbols. The pressure increases by 2 and 5% across the two weak shocks that are shown in Fig. 2. Also the entropy changes by 6% and the Mach number is reduced by a factor of 1.3 along the streamline. These shocks have also been observed experimentally in a Mach 6 boundary layer (Huntley, 2000).

The thickness of a shock is of the order of magnitude of the molecular mean free path λ_p. Figure 4 shows the ratio of the Kolmogorov scale η to λ_p. For the conditions chosen, λ_p is one to two orders of magnitude smaller than η. Today, the type of resolution required to resolve such a small length scale is not practical.

Figure 5 shows the instantaneous density contours in a streamwise-wall-normal plane given using a shock-capturing technique (Weirs & Candler, 1997) (a) and using a hybrid scheme (Olejniczak *et al.*, 1996) combining finite-difference and upwinding techniques (b). For the solution given by the hybrid scheme, the lack of shock-capturing capabilities generates noise near the boundary layer edge. As the simulation progresses in time, the numerical noise penetrates the boundary layer and the solution is no longer physical. Thus, a shock capturing technique is necessary for performing DNS and LES of hypersonic and supersonic boundary layers.

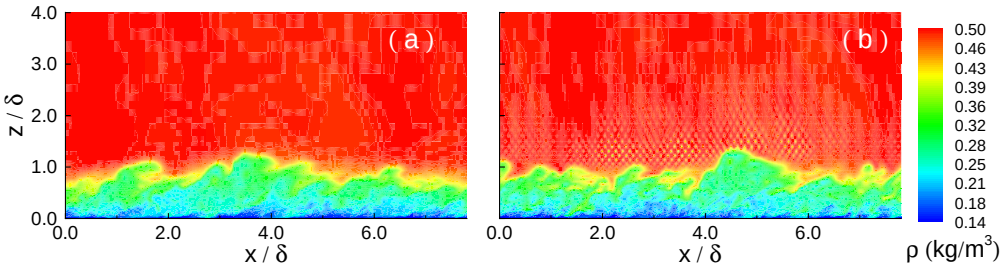

FIGURE 5. Density contours along a streamwise-wall-normal plane using an (a) shock-capturing technique and (b) no shock-capturing technique.

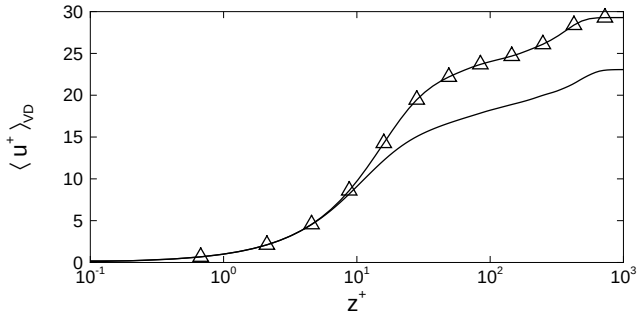

FIGURE 6. Van-Driest transformed velocity profile scaled on inner variables. ——, DNS; —△—, LES using WENO.

3.2. *Shock capturing and LES*

The weighted ENO scheme (Weirs & Candler, 1997) was designed for low dissipation. In smooth regions, the convective fluxes are represented using a symmetric, six-point stencil which provides third-order accuracy, high bandwidth, and low dissipation. In calculating the flux, a smoothness measurement allows the stencil to adapt in regions where the data is not smooth. The adaption mechanism selects a more dissipative, upwinded stencil to approximate steep gradients without introducing spurious oscillations.

Figure 6 shows the performance of the WENO scheme when it is used for DNS and LES. Whereas the DNS result is acceptable, the LES result is not good. The adaption mechanism does not distinguish shock waves from turbulence fluctuations on coarse grids. Thus, the WENO scheme provides too much dissipation when used in a LES.

If we could better predict the shock location on coarse grids, we could use no adaption in smooth regions and full adaption near shocks. In the following, the compressibility ratio is used to predict the shock location. Shock waves are a result of a compression. Thus, the increased dissipation across a shock wave must be associated with the compressible dissipation only. An index of the compressibility is given by

$$\chi = \frac{\langle\, |\nabla \cdot \mathbf{u}'|^2 \,\rangle}{\langle\, |\nabla \times \mathbf{u}'|^2 \,\rangle} \tag{3.3}$$

Thus, a jump in the compressibility ratio represents a jump in the dilatation and, therefore, the location of a shock. Figure 7 shows that near the boundary layer edge the compressibility ratio increases suddenly near $z/\delta = 1.25$.

Using the compressibility ratio to find the shock location and control the adaption

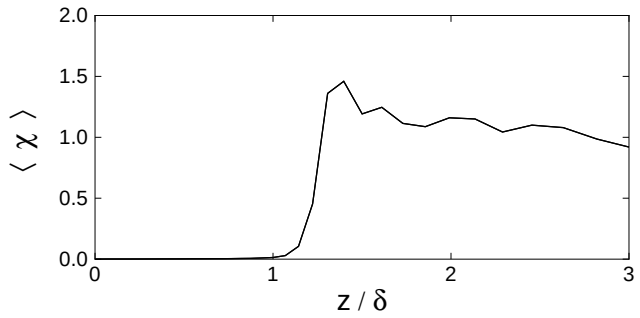

FIGURE 7. Relative compressible to incompressible energy ratio.

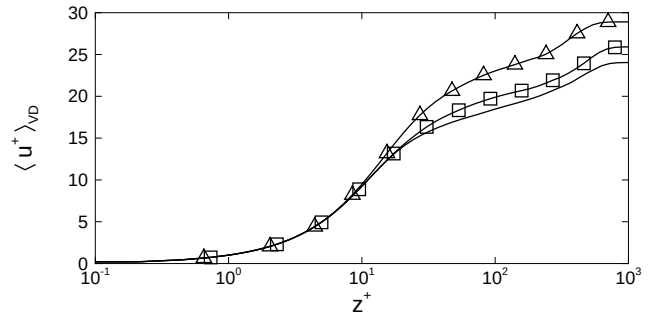

FIGURE 8. Van-Driest transformed velocity profile scaled on inner variables. ——— , DNS; —△— , WENO (25% error); —□— , LWENO (7% error).

mechanism decreases the dissipation significantly and gives more accurate predictions. Figure 8 plots the Van-Driest velocity versus the distance from the wall for the DNS, the WENO and the WENO using local shock-capturing, LWENO. The more sophisticated shock prediction mechanism decreases the error in the solution from 25% to 7%.

3.3. *Conclusions and future work*

The presence of shock waves in supersonic boundary layers has been illustrated. Since the required resolution to resolve shock waves is impractical, shock-capturing techniques are necessary for the DNS and LES of supersonic or hypersonic turbulent boundary layers. It is found that the information provided by the smoothness measurement is not enough to determine the shock location on coarse, LES grids. A new shock-location prediction is obtained using the compressibility ratio. The local WENO shock-capturing mechanism based on the compressibility ratio gives good predictions when performing LES of supersonic boundary layers. Ongoing work includes the application of this new shock-capturing technique to the LES of hypersonic flow configurations.

REFERENCES

CANDLER, G. V., WRIGHT, W. J. & MCDONALD, J. D. 1994 *Data-Parallel Lower-Upper Relaxation method for reacting flows. AIAA J.* **32**, 2380-2386.

HUNTLEY, M. B. 2000 *Transition on elliptic cones at Mach 8,* PhD thesis, Princeton University.

JIANG, G.-S. & SHU, C.-W. 1996 Efficient implementation of weighted ENO schemes. *J. Comp. Phys.* **126**, 202-228.

MARTÍN, M. P. & CANDLER, G. V. 2000 DNS of a Mach 4 Boundary Layer with Chemical Reactions. *AIAA Paper No. 00-0399.* Also *AIAA Paper No. 98-2817.*

MARTÍN, M. P., WEIRS, V. W., CANDLER, G. V., PIOMELLI, U., JOHNSON, H., & NOMPELIS, I. 2000a Toward the large-eddy simulation over a hypersonic elliptical cross-section cone. *AIAA Paper No. 00-2311.*

MARTÍN, M. P., CANDLER, G. V., PIOMELLI, U. 2000b Subgrid-scale models for compressible large-eddy simulations. *Theor. and Comp. Fluid Dyn.* **13**, 361-376.

OLEJNICZAK, D. J., WEIRS, V. G., LIU, J., & CANDLER, G. V. 1996 Hybrid finite-difference methods for DNS of compressible turbulent boundary layers. *AIAA Paper No. 96-2086.*

WEIRS, V. G. & CANDLER, G. V. 1997 Optimization of weighted ENO schemes for DNS of compressible turbulence. *AIAA Paper No. 97-1940.*